International Refrigeration and Air Conditioning Conference

School of Mechanical Engineering

2022

Improving Robustness of Transient Heat Exchanger Models with Non-uniform Frost Formation

Jiacheng Ma

Donghun Kim

James E. Braun

Improving Robustness of Transient Heat Exchanger Models with Non-uniform Frost Formation

Jiacheng Ma[1*], Donghun Kim[2], James E. Braun[1],

[1] Ray W. Herrick Laboratories, School of Mechanical Engineering, Purdue University,
West Lafayette, IN, U.S.
ma516@purdue.edu, jbraun@purdue.edu

[2] Building Technology & Urban Systems Division, Lawrence Berkeley National Laboratory,
Berkeley, CA, U.S.
donghunkim@lbl.gov

* Corresponding Author

ABSTRACT

Since frost accumulation is a common but undesired phenomenon for air-source heat pumps in winter operations, transient modeling of such systems with frost buildup on the evaporator coil is significantly useful for improved control designs under frosting conditions. Despite the abundance of modeling studies on heat exchanger behaviors under frosting operations, there still remain challenges on model robustness due to the complicated cycle dynamics coupled with frost dynamics. This paper presents a finite volume heat exchanger model with frost formation integrated into each control volume. A fan model is proposed to capture the air flow redistribution due to non-uniform frost formation on the coil surface, that can avoid solutions of a large nonlinear equation system, to improve the model robustness and numerical efficiency. The developed heat exchanger model is coupled to other component models to complete a heat pump cycle model. Transient simulations are carried out to explore the impact of frost on the system performance, and results are compared against experiment data.

1. INTRODUCTION

Frost formation occurs on evaporator coils typically when the surface temperatures are below the dew point of moist air and the freezing point of water during winter operations. As frost forms, decreases of the free air flow passage and increases of the thermal resistance between the surfaces and ambient air result in an overall degradation of the system performance, and potentially raise safety concerns. The buildup of frost eventually necessitates that the system shifts into a defrosting mode to remove the accumulated frost and return the system to its normal operating characteristics. For instance, reverse-cycle defrosting (RCD), that heats the outdoor coil by reversing the thermodynamic cycle, is one of the predominant defrost approaches for air-source heat pump (ASHP) units (Nawaz et al., 2018). Currently the most common defrost control strategy for ASHP and refrigeration systems is the time-based defrost, that initiates a defrost cycle after a pre-programmed time interval (Song et al., 2018). Since this strategy relies on open-loop operations or incorporates fairly simple feedback schemes (e.g., tube surface temperature of the outdoor coil) that can not reflect the actual operating characteristics, systems applying the strategy may suffer from considerable energy inefficiencies. Dynamic modeling of ASHP with frost buildup is extremely useful in development and evaluation of improved control, fault detection and diagnostics (FDD) algorithms. Furthermore, transient models that can capture the ASHP system dynamics under frosting conditions will facilitate optimizing the defrost interval to improve the overall system performance and minimize interruptions caused by defrost operations.

Due to the complicated underlying physical behaviors of coupled frost and refrigerant loop dynamics, a very limited number of system-level modeling efforts can be found in the open literature. Many studies solely focused on the heat exchanger air-side performance neglecting the refrigerant loop dyanmics, e.g., (Da Silva et al., 2011; Padhmanabhan et al., 2011; Breque & Nemer, 2016). In terms of complete cycle modeling studies considering the dynamics on both the refrigerant side and air side, Qiao et al. (2017) integrated a one-dimensional frost growth model into a segment-by-segment evaporator model coupled to other components of a two-stage flash tank vapor injection heat pump system. Transients of the system going through a start-up period, a stable frosting stage, followed by an unstable hunting

stage due to the performance degradation by frost accumulation were simulated. Comparisons of the simulation results against experimental data indicate that the developed model can reasonably predict the system responses under frosting conditions. The distributed-parameter heat exchanger model is able to capture the surface temperature variations along the refrigerant flow path due to pressure drop, and thus predict the non-uniform frost formation in each discretized unit. As a result, such a heat exchanger model coupled to a fan model can be used to solve the air flow distribution over time due to non-uniform frost thicknesses, also known as air flow maldistribution. Padhmanabhan et al. (2011) formulated a non-linear algebraic equation system based on the air pressure drop equalization to predict this phenomenon. Chung et al. (2019) and Breque and Nemer (2017) followed the same approach to compute the air flow distribution by numerical iterations. Qiao et al. (2017) proposed a simplified approach by linearizing the pressure drop equalization equations with respect to air mass flow rates of control volumes and the total fan volume flow rate, such that the time evolution of air flow redistribution can be computed in an explicit manner without numerical iterations. However, in order to perform the linearization, a symbolic system of pressure drop equalization equations needs to be formulated by substituting a specific fan curve as well as air pressure drop correlation into the equations. It is not straightforward to implement this approach to general ASHP systems, since a specific fan model needs to be developed when different fan curves or empirical pressure drop correlations are used. Furthermore, the approach cannot be easily implemented in an object-oriented modeling language such as Modelica. The objective of this work is to develop a general simulation tool for ASHP under frosting operations capable of captureing the dominant system transients and enables robust simulations for control and FDD purposes. To achieve this, a one-dimensional heat exchanger model integrated with frost formation is developed, and then coupled to other component models to complete a cycle model. Specifically, a fan model is proposed that avoids solution of a large non-linear algebraic system and is easy to adapt in an object-oriented way. The reminder of this paper will be presented as follows. Section 2 presents development of a complete ASHP cycle model for predicting system behaviors under frosting conditions. Section 3 reports simulation results and comparisons against the measurements, followed by a summary of conclusions in Section 4.

2. MODEL DEVELOPMENT

2.1 Heat Exchanger Model
Much of the previous modeling efforts have focused on heat exchanger models since the dominant dynamics of a general vapor compression cycle reside in two-phase heat exchangers. In the present work, a heat exchanger model is integrated with a detailed frost growth model to investigate the overall impact of frost formation on the system performance. To describe dynamics of the refrigerant in heat exchanges, a number of assumptions are required to simplify the model construction of two-phase flow:

- The refrigerant flow is one-dimensional with uniform fluid properties at cross sections.

- Changes in kinetic energy and potential energy are negligible; viscous dissipation is negligible; axial heat conduction along the refrigerant flow direction is negligible.

- The liquid and vapor of the two-phase region are in thermodynamic equilibrium.

- Body forces are neglected in the momentum balance.

The finite volume (FV) approach, that segments a heat exchanger into an arbitrary number of equally sized control volumes, is utilized for discretization. The refrigerant pressure and enthalpy as a pair of independent thermodynamic properties are chosen as state variables to express the discretized governing equations. A staggered grid scheme is adopted to solve the balance equations in those control volumes (Laughman et al., 2015). As shown in Figure 1, the mass and energy balances are solved in the upper grid, referred to as volume cells, where thermodynamic properties are determined, while the momentum balance is solved in the lower grid, referred to as flow cells, where dynamics of the mass flow rate are evaluated for neighboring volume cells. With a discretization of n control volumes for a heat exchanger, $n - 1$ momentum balances are formed, where each of the two boundary flow cells has an extended length of half the cell. In this way, the momentum balances solve interface mass flow rates on the $n - 1$ inner edges of the volume cells, leaving mass flow rates on the outer edges ($\dot{m}_1, \dot{m}_{n+1}$) as boundary conditions to the grid. Meanwhile, the first and last volume cells expose the thermodynamic states. As a result, connection with other flow devices avoids the solution of large nonlinear systems for algebraic pressures (Franke et al., 2009). The discretized governing equations
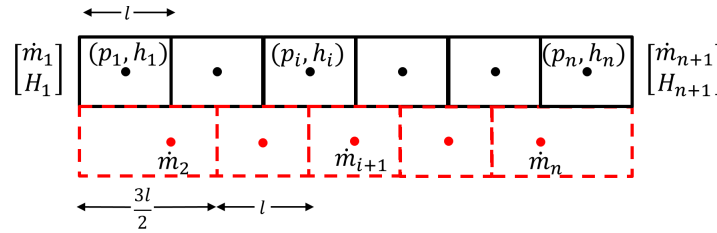
Figure 1: Staggered grid for discretization of balance equations.

of refrigerant mass, momentum and energy balances are given respectively in (1)-(3),

$$V\left[\left(\frac{\partial\rho}{\partial p}\Big|_h\right)_i\frac{dp_i}{dt} + \left(\frac{\partial\rho}{\partial h}\Big|_p\right)_i\frac{dh_i}{dt}\right] = \dot{m}_i - \dot{m}_{i+1} \tag{1}$$

$$L_i\frac{d\dot{m}_i}{dt} = \rho_{i-1}\bar{v}_{i-1}^2 A_{i-1} - \rho_i\bar{v}_i^2 A_i + \frac{A_{i-1} + A_i}{2}(p_{i-1} - p_i) - F_{f,i} \tag{2}$$

$$V\left[\left(h_i\frac{\partial\rho}{\partial p}\Big|_h - 1\right)_i\frac{dp_i}{dt} + \left(h_i\frac{\partial\rho}{\partial h}\Big|_p + \rho\right)_i\frac{dh_i}{dt}\right] = H_i - H_{i+1} + \dot{Q}_i \tag{3}$$

where V denotes the volume of each volume cell, L_i denotes the length of a flow cell, $\bar{v}_i$ denotes the average velocity of a volume cell, $F_{f,i}$ denotes the friction force across a flow cell which is evaluted by the equivalent frictional pressure drop, $\dot{Q}_i$ is the convective heat transfer rate with the metal wall, H_i denotes the enthalpy flow rate computed at the edge of a volume cell. The upwind difference scheme is used to approximate thermodynamic quantities at the volume cell interfaces. Therefore, the enthalpy flow rate can be calculated as

$$\begin{cases} H_i = \dot{m}_i h_{i-1,\text{upstream}} \\ H_{i+1} = \dot{m}_{i+1} h_i. \end{cases} \tag{4}$$

Assuming a uniform temperature of the tube wall and associated fins, conservation of energy for the coil metal structure can be derived as

$$\left(M_{fin}c_{p,fin} + M_t c_{p,t}\right)_i\frac{dT_{w,i}}{dt} = \alpha_{r,i}A_{s,i}(T_{r,i} - T_{w,i}) + \dot{Q}_{f,i} \tag{5}$$

where $\dot{Q}_{f,i}$ denotes heat conduction with the frost layer. The air temperature and humidity profile can be derived from one-dimensional, quasi-steady-state mass and energy balances with a uniform surface temperature and inlet air conditions,

$$T_{ai,out} = T_{as,i} + (T_{a,in} - T_{as,i})e^{-Ntu} \tag{6}$$

$$\omega_{ai,out} = \omega_{a,in} + \left(1 - e^{-\frac{Ntu}{Le^{2/3}}}\right)\max\{0, \omega_{a,in} - \omega_{as,i}\} \tag{7}$$

where Ntu is the number of transfer units for sensible heat transfer,

$$Ntu = \frac{\alpha_{a,i}(A_t + \eta_{fin}A_{fin})_i}{\dot{m}_{a,i}c_{p,a}} \tag{8}$$

$\omega_{as,i}$ is the saturated humidity ratio evaluated at the surface temperature $T_{as,i}$. The heat and mass transfer analogy through the Lewis number $Le^{2/3} = 0.9$ is adopted to correlate convection coefficients of heat and mass transfer, which is valid in both cases of condensation and sublimation (Bergman et al., 2011; Leoni et al., 2017). The total heat transfer consisting of sensible and latent parts can be obtained by

$$\dot{Q}_i = \dot{m}_{a,i}c_{p,a}(T_{ai,out} - T_{a,in}) + \dot{m}_{a,i}(\omega_{ai,out} - \omega_{a,in})\Delta h_{lat} \tag{9}$$

where Δh_{lat} represents the latent heat of condensation or sublimation according to the surface temperature.
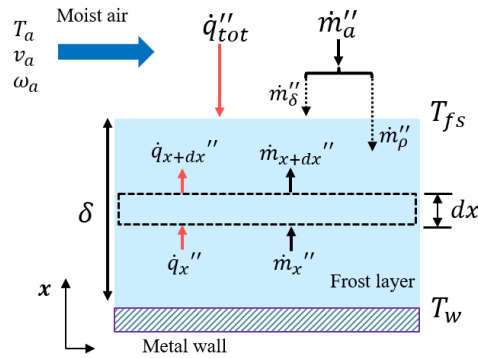
Figure 2: Schematic of one-dimensional frost growth.

The prediction of frost formation on the outdoor coil is essential to characterize the performance of an ASHP system under frosting conditions due to blockage of the air flow passage and additional thermal resistance. To make a numerical model tractable, it is often assumed that frost growth normal to the cold surface is of primary interest. The frost layer growth and densification rates can be determined by solving the heat and mass diffusion equations. As shown in Figure 2, at the frost-air interface, the total heat flux from the air stream is composed of sensible and latent heat due to the temperature and humidity differences,

$$q_{tot}^{''} = \alpha_h(T_a - T_{fs}) + \alpha_m(\omega_a - \omega_{fs})\Delta h_{sg} \tag{10}$$

where α_h denotes the heat transfer coefficient, α_m denotes the mass transfer coefficient, T_{fs} denotes the frost surface temperature, ω_{fs} denotes the saturated humidity ratio at the frost surface, Δh_{sg} denotes the water sublimation heat. Note that (10) represents the same heat transfer rate as (9) under frosting conditions. It also gives the amount of heat conducted to the metal structure ($\dot{Q}_{f,i}$) in (5), assuming that the frost growth process is quasi-steady-state. When the frost layer is of thickness $\delta_{f,i}$ and lumped density $\rho_{f,i}$, mass conservation of the frost layer can be formed as

$$\frac{d}{dt}(\rho_{f,i}\delta_{f,i}) = \alpha_{m,i}(\omega_{ai,in} - \omega_{fs,i}) = \dot{m}_{a,i}^{''} \tag{11}$$

which can rewritten as

$$\rho_{f,i}\frac{d\delta_{f,i}}{dt} + \delta_{f,i}\frac{d\rho_{f,i}}{dt} = \dot{m}_{\delta,i}^{''} + \dot{m}_{\rho,i}^{''}. \tag{12}$$

(12) indicates that the total water mass flux is divided into two components: $\dot{m}_{\delta}^{''}$ contributes to an increment of the frost thickness and $\dot{m}_{\rho}^{''}$, which is diffused into the frost layer, contributes to its densification. Consider a differential control volume of thickness dx within the frost layer as shown in Figure 2, the heat and mass diffusion can be formulated and then solved associated with boundary conditions at the wall surface and the frost-air interface. For the sake of brevity, the solution procedure is not included in the present paper. Refer to Qiao et al. (2017) for derivations to obtain the mass flux in (12). Since the model is derived following a quasi-steady-state assumption, the frost thickness and density are updated at a fixed time step Δt

$$\rho_{f,i}(t + \Delta t) = \rho_{f,i}(t) + \frac{\dot{m}_{\rho,i}^{''}}{\delta_{f,i}}\Delta t \tag{13}$$

$$\delta_{f,i}(t + \Delta t) = \delta_{f,i}(t) + \frac{\dot{m}_{\delta,i}^{''}}{\rho_{f,i}}\Delta t \tag{14}$$

which enables the overall frost growth process to remain transient over time. Note that (13) and (14) can be viewed as a discrete dynamical system. Since the refrigerant dynamics are described in a continuous-time domain, the overall heat exchanger model is characterized by a hybrid system, which cannot be solved efficiently. Therefore, the updated

values at each time interval are considered as reference values. Then a first-order filter is applied to track the reference values

$$\frac{d\rho_{f,i}}{dt} = \frac{1}{\tau}(\rho_{\text{ref},i} - \rho_{f,i}) \tag{15}$$

$$\frac{d\delta_{f,i}}{dt} = \frac{1}{\tau}(\delta_{\text{ref},i} - \delta_{f,i}) \tag{16}$$

where $\rho_{\text{ref},i}$ and $\delta_{\text{ref},i}$ are quantities evaluated in (13, 14), $\rho_{f,i}$ and $\delta_{f,i}$ are states representing the frost behavior, τ is a time constant, which should be selected such that the signal tracking is faster than update of the reference values.

2.2 Component Models

A quasi-static model is developed to describe performance of a variable-speed compressor using efficiency maps. The refrigerant mass flow rate is determined by

$$\dot{m} = \rho_{\text{suc}}\eta_v V_s \frac{N}{60} \tag{17}$$

where V_s is a fixed displacement, N is the number of rotations per minute, η_v is the volumetric efficiency. The power consumption is estimated using an isentropic efficiency

$$\eta_{is} = \frac{\dot{m}(h_{\text{dis,is}} - h_{\text{suc}})}{\dot{W}}. \tag{18}$$

The refrigerant discharge state can be determined by forming an energy balance for the compressor,

$$\dot{W} = \dot{m}(h_{\text{dis}} - h_{\text{suc}}) + f_q \dot{W}. \tag{19}$$

The efficiency maps of η_v, η_{is} and f_q are regressed by polynomials of pressure ratio, the compressor speed and the ambient temperature. The expansion process is assumed to be isenthalpic. The mass flow rate is determined by

$$\dot{m} = C_d A_v \sqrt{2\rho_{\text{in}}(p_{\text{in}} - p_{\text{out}})} \tag{20}$$

where A_v is the varying valve opening area, and C_d is the discharge coefficient that accounts for corrections to the mass flow rate at different operating conditions. The opening area is adjusted based on superheat control. An empirical correlation based on a power law is utilized to estimate the discharge coefficient (Liu et al., 2022):

$$C_d = d_0 \varphi^{d_1} \left(\frac{T_{\text{sc}}}{T_c}\right)^{d_2} \tag{21}$$

where $d_0 - d_2$ are constant coefficients, T_{sc} is the subcooling at the valve inlet, T_c is the critical temperature of the refrigerant, and φ is the normalized valve opening.

An accumulator is modeled assuming that vapor and liquid inside are saturated and in thermal equilibrium, which lead to the mass and energy conservation equations as shown in (22)-(23),

$$\frac{d}{dt}\left(V_g \rho_g + V_f \rho_f\right) = \dot{m}_{\text{in}} - \dot{m}_{\text{out}} \tag{22}$$

$$\frac{d}{dt}\left(V_g \rho_g u_g + V_f \rho_f u_f\right) = \dot{m}_{\text{in}} h_{\text{in}} - \dot{m}_{\text{out}} h_{\text{out}}. \tag{23}$$

Note that these saturated properties are solely dependent on the refrigerant pressure, thus the lumped pressure can be selected as a state variable. Given the constituent relation that the total volume of the tank is occupied by the saturated liquid and vapor volumes $V_f + V_g = V_{\text{acc}}$, either one of the volumes can be selected as another state variable. The exit flow is assumed to be saturated vapor to account for the fact that the superheated vapor from the evaporator mixes with the liquid refrigerant stored inside the accumulator. The coil fan is described via a polynomial characteristic curve:

$$\Delta p_{rise} = a_0 + a_1 \dot{V} + a_2 \dot{V}^2 + a_3 \dot{V}^3. \tag{24}$$

where $\dot{V}$ is the total volume flow rate. Since the coil pressure drop is assumed to be solely a result of friction, a hydraulic equilibrium is established between the fan and the coil, which leads to the system of equations below:

$$\Delta p_{rise} = \Delta p_{a,i} \quad i = 1, \ldots, N \tag{25}$$

where $\Delta p_{a,i}$ is the air side pressure drop of the ith control volume, as computed by empirical correlations (Wang et al., 2000). Along with the mass balance

$$\rho_a \dot{V} = \sum_{i=1}^{N} \dot{m}_{a,i} \tag{26}$$

where $\dot{m}_{a,i}$ represents the air flow distribution of each control volume, a non-linear algebraic equation system is formed to solve the air flow maldistribution under non-uniform frost formation. As stated previously, a computationally efficient and robust approach is desired. A new fan model is introduced based on a robust formulation of thermo-fluid streams proposed by (Zimmer, 2020). Denote an inertial pressure r:

$$-\frac{L}{A_s}\frac{d\dot{m}}{dt} = -\Delta r \tag{27}$$

where L is the flow path length, A_s is the flow area, and the term $I = \frac{L}{A_s}$ can be regarded as the inertance of the flow, which represents the reluctance of the mass flow to change, and acts as a time constant for the mass flow dynamics. Consider a general one-dimensional momentum balance

$$I\frac{d\dot{m}}{dt} + \rho\bar{v}\Delta v = -\Delta p - \Delta p_{ext} \tag{28}$$

where $\bar{v}$ is the average velocity of a control volume, Δp_{ext} is the equivalent pressure drop due to external forces (e.g., friction). By introducing a new term, the steady mass flow pressure $\hat{p}$ and a decomposition

$$p = \hat{p} + r \tag{29}$$

the equation in (28) can be rewritten as

$$\Delta\hat{p} = -\rho\bar{v}\Delta v - \Delta p_{ext}. \tag{30}$$

Note that the terms on the right hand side are dependent on the fluid pressure and mass flow rate. An approximation of evaluating those terms using the steady mass flow pressure $\hat{p}$ instead of p gives

$$\Delta\hat{p} = -\rho\bar{v}\Delta v(\dot{m}, \hat{p}) - \Delta p_{ext}(\dot{m}, \hat{p}). \tag{31}$$

This form indicates that when considering a momentum balance, if the state variable mass flow rate is evaluated through the difference of inertial pressures as given in (27) that controls acceleration or deceleration of the flow, then the downstream pressure can be explicitly computed if the upstream pressure is known. The same applies to other thermodynamic properties. Concerning a quasi-steady-state component model, this approach adds dynamics to the mass flow rate that is previously determined by algebraic functions of thermodynamic properties, that converts an algebraic equation system to an ordinary differential equation (ODE) system and avoids solving non-linear equation systems by numerical iterations. Implementation of this approach to a one-dimensional air flow distribution problem is depicted in Figure 3. Since mass flow rates of the fan and each control volume are now state variables, they can be considered known at each time step. Then thermodynamic properties are computed straightforwardly from source to sink. For instance, the pressure rise of the fan is computed using the fan curve given in (24), which further determines $\hat{p}_A$. Similarly, the pressure drop of each control volume can be calculated using the known mass flow rates, which gives $\hat{p}_1, \hat{p}_2, \cdots, \hat{p}_N$. In this case, pressures of the source and sink are set to the atmospheric pressure p_{atm}. It is shown in (Zimmer, 2020) that the mixing pressure $\hat{p}_B$ can be approximated as

$$\hat{p}_B = \frac{\sum_{i=1}^{N} \dot{m}_i \hat{p}_i}{\sum_{i=1}^{N} \dot{m}_i} \tag{32}$$

Figure 3: Computational scheme of the fan model.

based on the mass conservation at the mixing point B. With all the pressures in Figure 3 determined, the next step is to compute the inertial pressures and evaluate dynamics of the mass flow rates for integration over the next time step. The inertial pressures and mass flow dynamics can be obtained simultaneously by forming a system of ODEs and equations of pressure equalization:

$$-I_f \frac{d\dot{m}_f}{dt} = r_A$$

$$-I_1 \frac{d\dot{m}_1}{dt} = r_1 - r_A, \cdots, -I_N \frac{d\dot{m}_N}{dt} = r_N - r_A$$

$$\hat{p}_1 + r_1 = \hat{p}_B + r_B, \cdots, \hat{p}_N + r_N = \hat{p}_B + r_B$$

$$\hat{p}_B + r_B = p_{atm}. \tag{33}$$

The above system consists of $2N + 2$ equations but $2N + 3$ unknowns. To close the system, a derivative form of the mass balance is added

$$\frac{d\dot{m}_f}{dt} = \sum_{i=1}^{N} \frac{d\dot{m}_i}{dt}. \tag{34}$$

The equations can be rewritten in a matrix form:

$$
\begin{bmatrix}
-I_f & & & & -1 & & & \\
& -I_1 & & & 1 & -1 & & \\
& & \ddots & & & & \ddots & \\
& & & -I_N & 1 & & & -1 \\
& & & & 1 & & & -1 \\
& & & & & \ddots & & -1 \\
& & & & & & 1 & -1 \\
& & & & & & & 1 \\
1 & -1 & \cdots & -1 & & & &
\end{bmatrix}
\begin{bmatrix}
\frac{d\dot{m}_f}{dt} \\
\frac{d\dot{m}_1}{dt} \\
\vdots \\
\frac{d\dot{m}_N}{dt} \\
r_A \\
r_1 \\
\vdots \\
r_N \\
r_B
\end{bmatrix}
=
\begin{bmatrix}
0 \\
0 \\
\vdots \\
0 \\
\hat{p}_B - \hat{p}_1 \\
\vdots \\
\hat{p}_B - \hat{p}_N \\
p_{atm} - \hat{p}_B \\
0
\end{bmatrix}
\tag{35}
$$

which can be recognized without difficulty as a linear system. Note that this form is favorable because for most heat pump applications the equipment geometry is fixed, which indicates that the coefficient matrix on the left is a constant matrix. As a result, a linear time-invariant (LTI) system is formulated for the mass flow dynamics.

3. SIMULATION RESULTS AND VALIDATIONS

This section presents simulation results and experimental validations of the developed cycle model for capturing transient characteristics of a residential heat pump system under frosting. The heat pump unit is a commercial variable-speed system having a nominal capacity of 2 tons that utilizes R410A as the working fluid. The split system was installed in a pair of independently controlled psychrometric chambers, where the indoor unit was ducted to a nozzle

Figure 4: Validations of the refrigerant discharge and suction pressures.

box for air flow rate measurements. The temperature set points of the indoor and outdoor conditions were 291.5 K and 271 K, respectively. The relative humidity was set to 40% for the indoor and 85% for the outdoor. Each heat exchanger was discretized into 30 control volumes. The heat pump cycle model was simulated to predict system behaviors under multiple cycles of frosting and defrosting operations. Since this paper focuses on the frosting transients, especially the non-uniform frost formation on the evaporator coil, only the simulation results of a 2-hour heating operation in between defrost cycles are shown. The defrost dynamics are reported in a companion paper (Ma et al., 2022). Figure 4 reports validations of the refrigerant discharge and suction pressures. As the unit switches to the heating mode from the defrosting mode, the compressor speed increases to a desired setting regulated by the control board, which results in a rapid rise of the discharge pressure. After that, rise of the discharge pressure slows down since the compressor is running at a pre-defined speed. As the EXV is closing to achieve the superheat set point temperature, the resulting mass flow imbalance between the compressor and EXV leads to the continuing pressure increase, though frost starts to form shortly after the system switches back to heating mode. Performance degradation due to frost formation becomes more evident at about 60 min before initiation of the next defrost cycle. The reduced air flow due to frost blockage results in a slight decline of the evaporating pressure, yet a significant decline of the discharge pressure which is more sensitive to changes on the suction side. The predictions of discharge and suction pressures agree well with the measurements, which demonstrate that the developed cycle model is able to capture the complicated refrigerant dynamics under the frosting condition.
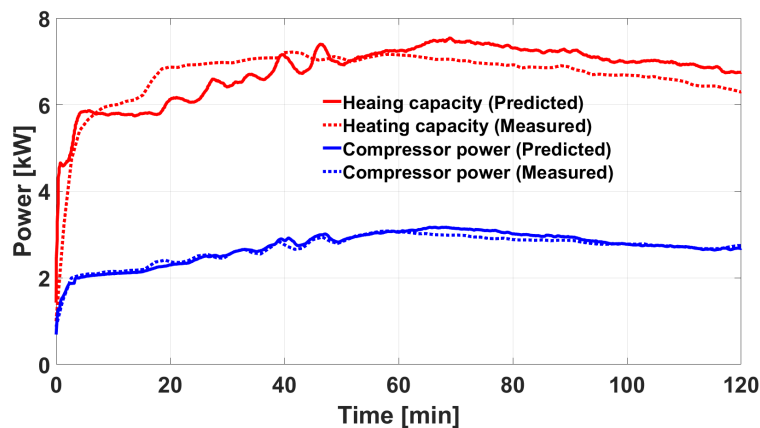
Figure 5: Validations of the indoor air-side capacity and compressor power.

Simulation results of the indoor unit air-side capacity and the the compressor power are shown in Figure 5. The indoor unit fan is continuously running throughout the test, and the air flow rate maintains a constant value based on the mea-
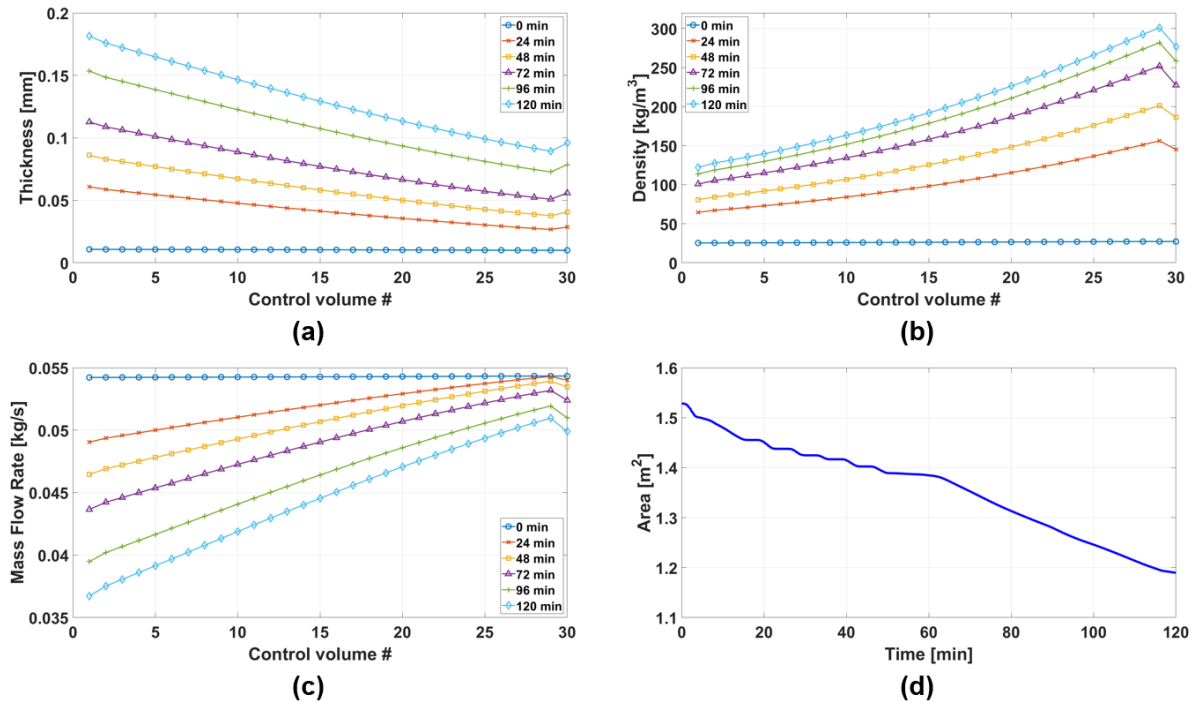
Figure 6: Simulated evolution of non-uniform frost growth: (a) Frost thickness; (b) Frost density; (c) Air mass flow rate; (d) Free air flow passage.

surements. The air-side capacity evolves corresponding to the refrigerant dynamics. As the condensing temperature climbs until 60 min, the heating capacity increases to the nominal capacity around 7 kW. Since the compressor operates at a nearly fixed speed, a decline of the heating capacity can be observed during 60 min to 120 min, when the refrigerant condensing pressure drops due to the frosting operation. Since the predictions of the refrigerant dynamics agree well with measurements, the model captures dynamics of the indoor capacities fairly well. The change of compressor power consumption follows regulation of the compressor speed, while also varying due to the refrigerant dynamics. During heating operations, the power consumption changes mainly due to transients of the discharge pressure, which in turn dominates the pressure ratio, as can be seen by the decline after 60 min which can be attributed to a smaller pressure ratio.

Simulation results associated with non-uniform frost growth are presented in Figure 6. Time evolution of the air mass flow rate along the evaporator coil illustrates the air flow maldistribution that as the heating operation progresses, a portion of the coil close to the refrigerant inlet receives less air flow than the portion close to the exit due to frost deposition. Moreover, the decline of the total air flow rate is caused by increased pressure drop across fins due to narrowed flow area, according to the fan curve. The air flow maldistribution, as a consequence, further stimulates the non-uniform frost growth on the coil, as shown by the simulated evolution of frost thickness and density. It can be noted from the total free air flow area that 23% of the flow passage is blocked after two hours of frosting operation.

4. CONCLUSIONS

This paper presents a dynamic modeling framework for air-source heat pumps with non-uniform frost formation on the evaporator coil. In particular, a fan model that avoids solutions of a nonlinear algebraic equation system to predict the air flow maldistribution, is proposed to improve the model robustness. The developed model was simulated to predict transients of a residential heat pump unit under frosting conditions. Agreement between the model predictions and measurements demonstrates that the model can capture the system performance degradation due to frosting operations. Furthermore, predictions of the time evolution of frost properties and air flow redistribution can help gain insights into the non-uniform frost formation phenomena and its impact on coil heat transfer, which are typically difficult to measure and characterize experimentally at a system level.

NOMENCLATURE

α	Heat transfer coefficient	$[\mathrm{W/(kg\,K)}]$
$\dot{m}$	Mass flow rate	$[\mathrm{kg/s}]$
ρ	Density	$[\mathrm{kg/m^3}]$
A	Area	$[\mathrm{m^2}]$
c_p	Specific heat capacity	$[\mathrm{J/(kg\,K)}]$
h	Specific enthalpy	$[\mathrm{J/kg}]$
M	Mass	$[\mathrm{kg}]$
p	Pressure	$[\mathrm{Pa}]$
T	Temperature	$[\mathrm{K}]$

Subscript

r	Refrigerant
a	Air
dis	Discharge
suc	Suction

REFERENCES

Bergman, T. L., Incropera, F. P., DeWitt, D. P., & Lavine, A. S. (2011). *Fundamentals of heat and mass transfer*. John Wiley & Sons.

Breque, F., & Nemer, M. (2016). Frosting modeling on a cold flat plate: Comparison of the different assumptions and impacts on frost growth predictions. *International Journal of Refrigeration*, *69*, 340–360.

Breque, F., & Nemer, M. (2017). Modeling of a fan-supplied flat-tube heat exchanger exposed to non-uniform frost growth. *International Journal of Refrigeration*, *75*, 129–140.

Chung, Y., Yoo, J. W., Kim, G. T., & Kim, M. S. (2019). Prediction of the frost growth and performance change of air source heat pump system under various frosting conditions. *Applied Thermal Engineering*, *147*, 410–420.

Da Silva, D. L., Hermes, C. J., & Melo, C. (2011). First-principles modeling of frost accumulation on fan-supplied tube-fin evaporators. *Applied Thermal Engineering*, *31*(14-15), 2616–2621.

Franke, R., Casella, F., Sielemann, M., Proelss, K., & Otter, M. (2009). Standardization of thermo-fluid modeling in modelica. fluid. In *Proceedings of the 7th international modelica conference* (pp. 122–131).

Laughman, C. R., Qiao, H., Aute, V., & Radermacher, R. (2015). A comparison of transient heat pump cycle models using alternative flow descriptions. *Science and Technology for the Built Environment*, *21*(5), 666–680.

Leoni, A., Mondot, M., Durier, F., Revellin, R., & Haberschill, P. (2017). Frost formation and development on flat plate: Experimental investigation and comparison to predictive methods. *Experimental Thermal and Fluid Science*, *88*, 220–233.

Liu, H., Cai, J., & Kim, D. (2022). A hierarchical gray-box dynamic modeling methodology for direct-expansion cooling systems to support control stability analysis. *International Journal of Refrigeration*, *133*, 191–200.

Ma, J., Kim, D., & Braun, J. E. (2022). Dynamic modeling of air source heat pumps under reverse-cycle defrosting. *19th International Refrigeration and Air Conditioning Conference at Purdue, July 10-14, 2022*.

Nawaz, K., Elatar, A. F., & Fricke, B. A. (2018). A critical literature review of defrost technologies for heat pumps and refrigeration systems.

Padhmanabhan, S., Fisher, D., Cremaschi, L., & Moallem, E. (2011). Modeling non-uniform frost growth on a fin-and-tube heat exchanger. *International journal of refrigeration*, *34*(8), 2018–2030.

Qiao, H., Aute, V., & Radermacher, R. (2017). Dynamic modeling and characteristic analysis of a two-stage vapor injection heat pump system under frosting conditions. *International Journal of Refrigeration*, *84*, 181–197.

Song, M., Deng, S., Dang, C., Mao, N., & Wang, Z. (2018). Review on improvement for air source heat pump units during frosting and defrosting. *Applied energy*, *211*, 1150–1170.

Wang, C.-C., Chi, K.-Y., & Chang, C.-J. (2000). Heat transfer and friction characteristics of plain fin-and-tube heat exchangers, part ii: Correlation. *International Journal of Heat and mass transfer*, *43*(15), 2693–2700.

Zimmer, D. (2020). Robust object-oriented formulation of directed thermofluid stream networks. *Mathematical and Computer Modelling of Dynamical Systems*, *26*(3), 204–233.